Industrial Crops & Products 233 (2025) 121335

Contents lists available at ScienceDirect

Industrial Crops & Products

journal homepage: www.elsevier.com/locate/indcrop

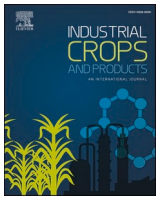

Sustainable poly(vinyl alcohol)/chitosan electrospun nanofibers and casted films with bioactive additives – comparative study on physicochemical properties and *in vitro* biological activity

Julia Kulczyńska [a,b,1], Vadym Chibrikov [c,2], Dominika Pawcenis [a,3], Roman J. Jędrzejczyk [d,4], Victor Sebastian [e,f,g,h,5], Justyna Cybulska [c,6], Artur Zdunek [c,7], Agnieszka Kyzioł [a,*,8]

[a] *Faculty of Chemistry, Jagiellonian University, Gronostajowa 2, Kraków 30-387, Poland*
[b] *Doctoral School of Exact and Natural Sciences, Jagiellonian University, Łojasiewicza 11, Kraków 30-348, Poland*
[c] *Institute of Agrophysics, Polish Academy of Sciences, Doświadczalna 4, Lublin 20-290, Poland*
[d] *Malopolska Centre of Biotechnology, Jagiellonian University, Gronostajowa 7A, Kraków 30-387, Poland*
[e] *Instituto de Nanociencia y Materiales de Aragón (INMA), CSIC-Universidad de Zaragoza, Zaragoza 50009, Spain*
[f] *Department of Chemical and Environmental Engineering Universidad de Zaragoza Campus Rio Ebro, Zaragoza 50018, Spain*
[g] *Networking Research Center on Bioengineering, Biomaterials and Nanomedicine, CIBER-BBN, Madrid 28-029, Spain*
[h] *Laboratorio de Microscopías Avanzadas, Universidad de Zaragoza, Zaragoza 50018, Spain*

A R T I C L E I N F O

Keywords:
Chitosan
Poly(vinyl alcohol)
Electrospinning
Nanofibers
Films
Antibacterial activity
Cytotoxicity

A B S T R A C T

Chitosan is a biocompatible and biodegradable polysaccharide with a plethora of biomedical and food applications. Its functionalization with additional biopolymers and bioadditives allows to modify its antimicrobial, mechanical and tribological properties, as well as cell proliferation. Thus, the aim of this study was to investigate the physicochemical properties and *in vitro* biological activity of poly(vinyl alcohol)/chitosan electrospun nanofibers and casted films with an addition of *Rosa damascena* and *Rosa rugosa* extracts, as well as gold nanoparticles. Poly(vinyl alcohol)/chitosan nanofibers and films were both electrospun and dry-casted with morphology, wettability, mechanical, thermal, antimicrobial properties, as well as cytotoxicity being examined. Specific attention has been drawn to the methodological approach on nanofiber electrospinning. Results showed data variabilities in wettability, mechanical and thermal properties were a matter of material fabrication technique, while those of swelling ability and degradation related to material composition. Antimicrobial activity, as well as lack of significant cytotoxicity were observed for both poly(vinyl alcohol)/chitosan nanofibers and films with an addition of rose extracts, as well as gold nanoparticles. Results reported in this study suggested poly (vinyl alcohol)/chitosan nanofibers and films with the investigated additives as promising biocompatible biomaterials with potential applications suggested such as external drug delivery in wound healing, topical therapies, biodegradable packings.

* Corresponding author.
E-mail addresses: julia.kulczynska@doctoral.uj.edu.pl (J. Kulczyńska), v.chibrikov@ipan.lublin.pl (V. Chibrikov), pawcenis@chemia.uj.edu.pl (D. Pawcenis), roman.jedrzejczyk@uj.edu.pl (R.J. Jędrzejczyk), victorse@unizar.es (V. Sebastian), j.cybulska@ipan.lublin.pl (J. Cybulska), a.zdunek@ipan.lublin.pl (A. Zdunek), kyziol@chemia.uj.edu.pl (A. Kyzioł).
[1] https://orcid.org/0009-0002-0218-1207
[2] https://orcid.org/0000-0002-2007-3800
[3] https://orcid.org/0000-0002-0406-4496
[4] https://orcid.org/0000-0002-1776-1784
[5] https://orcid.org/0000-0002-6873-5244
[6] https://orcid.org/0000-0003-3323-4535
[7] https://orcid.org/0000-0001-9395-1486
[8] https://orcid.org/0000-0002-5563-4508

https://doi.org/10.1016/j.indcrop.2025.121335
Received 14 April 2025; Received in revised form 27 May 2025; Accepted 6 June 2025
Available online 19 June 2025

1. Introduction

Nowadays, biopolymer materials, that can replace conventional plastics and non-renewable matter, are the main proposed alternatives defined in the actual strategy of the United Nations' Sustainable Development Goals (United Nations). For decades, the scientific community has focused on multiple compositional and methodological approaches in biomaterial production regarding the needs of the food packaging industry, textiles manufacturing, bioelectronics production, the niche of medical supplies, etc (Perveen et al., 2023). Current trends consider plant (cellulose, hemicellulose, pectin, lignin, alginate, xanthan, dextran) and animal (chitin, chitosan, collagen, silk) polysacharides as integral compositional elements of biomaterials, with films, hydrogels, patches, coatings, foams, membranes, nano- and macro-scaffolds as its form-factors (Toker-Bayraktar et al., 2023).

Chitosan is the second most abundant polysaccharide in Nature and is a cationic derivative of deacetylated chitin (Budiarso et al., 2023). Chitosan is produced from renewable sources, mainly from waste-derived feedstock from the food industry, such as crab, shrimp, and prawn shells (Natolino et al., 2025). Biocompatibility, biodegradability, adsorption capacity, and nontoxicity are among the crucial properties of chitosan applicability (Martau et al., 2019). In addition, its structural similarity to glycosaminoglycans in an extracellular matrix, such as hyaluronic acid and chondroitin sulfate, makes chitosan a promising candidate as a scaffold for biomedical and food applications (Kikani et al., 2024), (Alotaibi et al., 2023), (Rakkan et al., 2025), (Wang et al., 2025).

What is crucial is that the formation of chitosan nanoscaffolds is significantly limited by its polycationic nature, rigid backbone conformation, sparse chain entanglement, and strong intra- and intermolecular hydrogen bonding (Taokaew and Chuenkaek, 2024). Moreover, toxic solvents, such as trifluoroacetic acid and hexafluoroisopropanol are often used to handle chitosan spinability (Xu et al., 2009). To address the issue, blending with other polymers exhibiting high electrospinning properties is worth attention. Polymers that have been extensively used to enhance the spinability of chitosan comprise polyethylene oxide (Amiri et al., 2020), poly(vinyl alcohol) (Kulkarni et al., 2017), hyaluronic acid (Sun et al., 2019), polylactic acid (Chuah et al., 2023) due to its biocompatibility, biodegradability and lack of immunogenic effects.

With a clear path on the development of chitosan-based nanoscaffolds, the field of its application is a matter of modifications implemented. For instance, modification with Au, Ag, Cu nanoparticles (NPs) and essential oils contributes to antimicrobial activity of chitosan-based nanoscaffolds (Mohamady Hussein et al., 2020); crosslinking agents ensure their mechanical strength; graphene and silica enhance their thermal stability (Garnica-Palafox and Sánchez-Arévalo, 2016); plasticizers/antiplasticizers can modify wettability and moisture retention (Pinto et al., 2018); etc. In that way, incorporation of plant extracts in designing of an advanced biomaterials allows to ensure a set of unique properties, such as self-healing, underwater adhesion, stimuli responsiveness, antimicrobial activity, reversible/irreversible interactions, etc (Michalicha et al., 2024). *Rosa damascena* (RD) and *Rosa rugosa* (RR) are examples of natural resources rich in polyphenols, flavonoids, terpenes, phenolic acids, and other compounds (Akram et al., 2020), (Cendrowski et al., 2020). Rose extracts offer various documented effects such as analgesic, anticonvulsive, hypnotic, cardiovascular, laxative, anti-diabetic, antimicrobial, antioxidant, etc (Wang, 2024). Detailed biological activity of the components of rose extract is associated with multifaceted antitumor effectiveness, including modulation of pathways associated with cell proliferation, migration, angiogenesis, metastasis, and cell death (Mishra et al., 2022).

The research described in this article aimed to provide a comparative analysis on physicochemical properties and *in vitro* biological activity of chitosan/poly(vinyl alcohol) casted films and electrospun nanofibers with an addition of *Rosa damascena* and *Rosa rugosa* extracts, as well as gold nanoparticles. The morphology of chitosan/poly(vinyl alcohol) casted films and electrospun fibers, their wettability, swelling ability, molecular, thermal and mechanical properties, as well as their cytotoxicity and antimicrobial activity as a matter of material composition and fabrication were precisely investigated. Special attention was paid to the design and optimization of fabrication processes of chitosan/poly (vinyl alcohol) casted films and electrospun nanofibers with the addition of *Rosa damascena* and *Rosa rugosa* extracts. Moreover, gold nanoparticles, obtained with the application of *Rosa damascena* extract were introduced to check their additive effect on the physicochemical properties and biological activity of the investigated materials.

The basic materials presented herein are based on chitosan (a polymer of natural origin) and poly(vinyl alcohol) (a synthetic polymer), so that opens the possibilities for new proofs-of-concept concerning biodegradable while biocompatible materials containing also low-molecular-weight compounds of natural origin or supplemented with gold nanoparticles. Thus, these organic-inorganic hybrid materials produced according to the proposed sustainable way are a new generation of reproducible materials with potential biological applications. Noteworthy, both the material synthesis path and biodegradability are in line with the "green chemistry" approach. To the best of our knowledge, few publications are comparing morphologically diverse materials with different dimensionality in the nanoscale: fibers (1D) *versus* films (2D) with the same chemical composition in terms of their wettability, mechanical and thermal properties as well as biological response towards eukaryotic and prokaryotic cells *in vitro*. Furthermore, this study is an only integrated analysis of the effect *Rosa damascena* and *Rosa rugosa* extracts on physicochemical properties and *in vitro* biological activity of chitosan-poly(vinyl alcohol) casted films and the corresponding electrospun nanofibers.

2. Materials and methods

2.1. Materials and reagents

Shrimp shell chitosan (CSM), with a weight average molecular weight (M_w) of 127 ± 8 kDa and degree of deacetylation of 89 ± 2 % (Krajewska et al., 2011), as well as poly(vinyl alcohol) (PVA) with M_w of 89–98 kDa and a degree of hydrolysis of 99.0 % were purchased from Merck Group (Germany). Other reagents, used in the current study were of analytical grade and also purchased from Merck Group (Germany). For films and nanofibers preparation, CSM flakes were dissolved in 0.1 M acetic acid at 65 ± 1 °C overnight to obtain a 2 wt% stock solution. Poly(vinyl alcohol) was dissolved in deionized water at 90 ± 1 °C, to obtain 12 wt% stock solution.

2.2. Extraction of Rosa damascena (RD) buds and Rosa rugosa (RR) petals

Dried buds of RD and petals of RR sourced from a local herbalist's shop, originating from Morocco, were used in the study. A sample of 400 mg of dry RD buds (petals and stamens) or RR petals were mixed with distilled water to achieve a final concentration of 10 mg/mL. The aqueous extracts were prepared by stirring the mixtures for 60 min at 40 ± 1 °C. After allowing the mixtures to cool, the solutions were filtered using a syringe filter with a 0.22 μm pore size. The resulting extracts were stored in the dark at 21 ± 1 °C and used within a maximum of 7 days.

2.3. Synthesis of Au@RD nanoparticles and its characterisation

The synthesis of Au@RD nanoparticles (Au@RD NPs) was performed according to a previously described method (Kyzioł et al., 2021). Briefly, the reduction of Au(III) was initiated by adding 2 mL of a 5 mM aqueous solution of tetrachloroauric(III) acid to 18 mL of an aqueous RD extract at a concentration 1 mg/mL resulting in a final concentration of 0.5 mM

tetrachloroauric(III) acid in the reaction mixture. Then, the reaction mixture was stirred continuously at 90 ± 1 °C, whereby a pink color was developed within 3 min indicating the onset of Au@RD NPs formation.

2.4. Chitosan-poly(vinyl alcohol) film casting

Blends were prepared in advance by thoroughly mixing overnight at 21 ± 1 °C. Prior to mixing, pH of CSM solution was adjusted to 6 (pK_a(CSM) = 6.30). Then, the particular mixtures were cast into high impact polystyrene hexagonal molds, and left drying at 21 ± 1 °C and 40 ± 5 % relative humidity (RH) for 24 h. After that, PVA/CSM-based films were thermally stabilized at 130 ± 1 °C for 1 h. Such a treatment of common to decrease of solubility due to the initiated PVA-CSM cross-linking and anti-plasticizing effect (Zakrzewska et al., 2023). After thermal treatment, the casted films were peeled off from the molds and stored in sealed containers in dark at 21 ± 1 °C and 40 ± 5 % RH. The composition of the polymer blends, and sample codenames are shown in Table 1.

2.5. Chitosan-poly(vinyl alcohol) nanofiber electrospinning

Similarly to films, polymer blends for electrospinning were prepared in advance by thoroughly mixing overnight at 21 ± 1 °C. Electrical conductivity and viscosity of PVA/CSM-based blends were determined by SevenCompact S230 conductivity meter (Mettler Toledo, USA) and SV-10 viscometer (A&D Company Ltd., Japan), respectively, with data reported as Fig.S1 in Supplementary Materials. A Fluidnatek LE-50 (Fluidnatek, Spain) electrospinner with temperature and humidity control unit, equipped with a 21 G needle, was used to obtain nanofibers according to electrospinning parameters, provided in Table 1. The distance between the end of the needle and the collector plate was fixed at 13 cm. All nanofibers were obtained at 21 ± 1 °C and 40 ± 5 % RH. Following electrospinning, PVA/CSM-based nanofibers were thermally stabilized at 130 ± 1 °C for 1 h.

2.6. Scanning electron microscopy imaging

Scanning electron microscopy (SEM) imaging was performed using an Inspect F50 microscope (FEI) operated at an accelerating voltage of 15 kV. The maximum beam current was set to 200 nA, with a resolution of 20 nm under high vacuum conditions. The sample stage allowed for movement along the X, Y, and Z axes (50 × 50 × 50 mm) with tilt angles ranging from −15° to 75° and 360° rotation. Prior to analysis, the samples were sputter-coated with a thin layer of palladium to enhance surface conductivity and minimize charging effects during imaging. The real diameters of the fibers was determined by analysis of SEM images in the commercially available ImageJ program. Each time over 100 fibers from different microscopic images of the same sample were analyzed.

Table 1
Composition of polymer blends for film casting and nanofiber electrospinning, and parameters and nanofiber electrospinning process.

Codename	Composition	Electrospinning parameters	
		Voltage (kV)	Flowrate (mL/h)
PVA/CSM	PVA: 14 mL of 12 % w/v solution CSM: 4 mL of 2 % w/v solution dH_2O: 2 mL	22	0.5
PVA/CSM/RD	PVA: 14 mL of 12 % w/v solution CSM: 4 mL of 2 % w/v solution RD: 2 mL of 4 % w/v solution	21	0.5
PVA/CSM/RR	PVA: 14 mL of 12 % w/v solution CSM: 4 mL of 2 % w/v solution RR: 2 mL of 4 % w/v solution	21	0.5
PVA/CSM/ Au@RD NPs	PVA: 14 mL of 12 % w/v solution CSM: 4 mL of 2 % w/v solution Au@RD colloid: 2 mL of 4 % w/v solution	25	0.4

2.7. Raman spectra

Exploration of the molecular properties of PVA/CSM-based casted films and electrospun nanofibers was conducted according to the protocol reported previously (Chibrikov et al., 2023). Raman spectra were recorded using the alpha300R confocal Raman microscope (WITec, Germany) in single spectra mode at a temperature of 19 ± 1 °C and 33 ± 2 % RH. The Raman microscope wavelength of 532 nm at a power of 10 mW was used for excitation through the EC Epiplan-Neoflural 100X objective (Zeiss, Germany). For each sample, 5 spectra were acquired at random points over the range 4000 cm^{-1} - 150 cm^{-1} with a spectral resolution of 2.1 cm^{-1} Raman shift. Spectral data analysis was carried out using *ChemoSpec* R package, and included Savitzky-Golay smoothing, baseline correction with asymmetric least squares technique, and spectra normalization using the probabilistic quotient normalization method. Normalized Raman spectra were processed for principal component analysis (PCA) to reduce data dimensionality.

2.8. Mechanical properties

Macroscale mechanical properties of the samples were determined by means of a uniaxial tensile test with a constant strain rate. Material strips of an approximate length of 25 ± 3 mm, width of 3.0 ± 0.5 mm, and thicknesses of 0.02 ± 0.01 mm (electrospun nanofibers) and 0.12 ± 0.01 mm (casted films), were stored in a desiccator for at least 72 h at a 21 ± 1 °C and 25 ± 3 % RH prior further analysis. Mechanical testing was performed using a tensile stage microtester (Deben Microtest, UK) equipped with a 200 N load cell. In laboratory tests, samples were mounted in a way giving 10 mm as an effective length of a stripe, capable of stretching. Specimens were subjected to stretching with a constant strain rate of 1 mm/min up to 10 mm (100 %) deformation with 10 repetitions for each sample type. The Young's modulus of the sample was calculated according to Eq. (1):

$$E = \frac{l_0 \times s}{w \times t} \quad (1)$$

where E is Young's modulus of sample (MPa), l_0 is initial length of sample (mm), s is inclination of an elastic region slope, w is sample width (mm), and t is sample thickness (mm).

The experimental stress-strain curve may be found in Fig.S4 of the Supplementary Materials.

2.9. Wettability, swelling ability and degradation

The wettability of both nanofibers and films was evaluated through automatic contact angle measurement using a DSA25E goniometer (KRÜSS, Germany) by the double sessile drop method using 2 µL liquid drops (ultrapure distilled water). The contact angle was calculated as an average of at least 20 measurements. Surface free energies (SFE) were calculated as dispersive (γ_d) and polar (γ_p) components using the Owens-Wendt-Rabel-Kaelble method. By polar SFE component γ_p, the sum of the intermolecular interaction (polar, hydrogen, induction, acid–base, etc.) contributors were considered, while dispersion was considered as dispersive SFE component γ_d. Measurements were conducted in triplicate at 21 ± 1 °C and 40 ± 5 % RH.

Swelling ability and degradation of PVA/CSM-based nanofibers and films were investigated by sample incubation in phosphate buffered saline (PBS, pH = 7.4) at 37 ± 1 °C to mimic the physiological conditions of the human body. The samples with the weight of approximately

50 mg were placed in separate vessels on a horizontal shaker operating at 110 rpm. During the assay, the PBS volume was maintained constant. For *in vitro* swelling test, samples were weighed at the beginning of the experiment (0 h) and again after 1 h, 1 day, 7 days, and 14 days of incubation. Swelling ability was calculated according to Eq. (2):

$$Swelling\ ability[\%] = \frac{W_i - W_0}{W_0} \times 100\% \quad (2)$$

where W_i is the weight of the swollen sample after a particular incubation time (mg), W_0 is the weight of dried sample before incubation (mg).

For *in vitro* degradation test, samples were weighed at the beginning of the experiment and again after 1 day, 7 days, and 14 days of incubation. After each time interval, samples were dried at 37 ± 1 °C for 3 days prior weighting. Mass loss of each sample was calculated according to Eq. (3):

$$Weight\ loss[\%] = \frac{W_0 - W_i}{W_0} \times 100\% \quad (3)$$

where W_0 is the weight of the sample before incubation and W_i is the weight of the dried sample after incubation.

2.10. Thermal properties

For calorimetric analysis, 2.0 ± 0.2 mg of sample pieces were sealed in aluminium crucibles (TA Instruments, USA). Prior to analysis, samples were stored in a desiccator for at least 72 h at 21 ± 1 °C and 25 ± 3 % RH. Calorimetric analysis was conducted by means of differential scanning calorimetry (DSC) using DCS 250 differential scanning calorimeter (TA Instruments, USA). The experimental setup included sample heating in a temperature range of 20–400 ºC with a heating rate of 10 ºC×min^{-1} and nitrogen gas flux of 50 mL×min^{-1}. At the defined conditions, the limitation of heat transfer inside the material and in the external gas phase is negligible. Prior to the experiment, temperature and heat flow calibration of the equipment was done with indium under similar conditions as for samples.

Specific enthalpies were calculated according to the Eq. (4):

$$\Delta H = \int_{T_{start}}^{T_{end}} \frac{dQ}{dt} dt \quad (4)$$

where ΔH is specific enthalpy, (J/g), T_{start} is time of exo-/endotherm start (s), T_{end} is time of exo-/endotherm end (s), $\frac{dQ}{dt}$ is normalized heat flow (W/g), dt – integration time (s).

Temperatures and enthalpies of surface water evaporation and material decomposition were evaluated with TRIOS software (TA Instruments, USA) analysis tools. Experimental thermogram of casted CSM film can be found in Fig.S5 of the Supplementary Materials.

2.11. Antioxidant activity

To assess the scavenging potential of RD and RR extracts, Au@RD NPs, PVA/CSM nanofibers and films, 2,2-diphenyl-1-picrylhydrazyl (DPPH) assay was used according to the adopted spectroscopic method of Brand-Wiliams (Javed et al., 2023). An ethanol solution of quercetin at a final concentration of 1 mg/mL was used as a reference antioxidant. Respectively, to 20 mL of reference solution, RR or RD extract (40 mg/mL), Au@RD NPs (1 mL of the freshly prepared colloid diluted to 20 mL), 1.5 mL of 0.2 mg/mL DPPH solution in ethanol were added. Then, 1 × 1 cm sample pellicles were placed in 20 mL of distilled water containing 1.5 mL of 0.2 mg/mL DPPH solution in ethanol. The mixtures were kept aside on the magnetic stirrer in the dark for 30 min to complete the reaction. Then, absorbance was measured at 517 nm against an equal amount of DPPH and ethanol as a blank. The percentage of DPPH$^{\bullet}$ scavenging was estimated using the Eq. (5):

$$DPPH^{\bullet}\ scavenging[\%] = \frac{A_0 - A_1}{A_0} \times 100\% \quad (5)$$

where A_0 is the absorbance of the reference sample and A_1 is a sample absorbance.

2.12. Evaluation of in vitro biocompatibility – cell attachment and proliferation assays

HaCaT cells (epidermal human keratinocyte, CSL, Germany) were cultured on PVA/CSM-based samples. Scaffold materials were cut into 1 × 1 cm squares and sterilized by quick immersion in 70 % (v/v) ethanol, followed by washing with phosphate-buffered saline (PBS) in triplicate. The procedure was repeated in triplicate and samples were then put into 12-well culture plates. Approximately 3 × 10^4 cm cells were seeded directly on each sample. Then, cells were cultured in Dulbecco's modified eagle medium (DMEM) supplemented with 1 % (v/v) fetal bovine serum and 1 % (v/v) penicillin/streptomycin and incubated at 37 ± 1 °C under a humidified atmosphere of 5 % (v/v) carbon dioxide for 1 day and 3 days. The medium was changed for a fresh one every other day. Cells cultured on polystyrene culture plates (Corning, USA) were treated as a reference sample. After 1 day and 3 days, cytotoxicity was determined by Alamar Blue assay (Sigma-Aldrich, USA). In brief, cells were washed with PBS and incubated with resazurin sodium salt solution (25 μM in PBS) for 4 h at 37 ± 1 °C in the dark. The fluorescence associated with the cellular metabolic activity was measured at 605 nm (excitation wavelength 560 nm) with a multimode microplate reader (Infinite 200 M PRO NanoQuant, Tecan, Switzerland). Cytotoxicity was expressed as a percentage of viable cells after treatment with films and fibers in reference to untreated cells (control). The experiment was repeated in triplicate.

The adhesion and morphological changes of HaCaT cells on nanofibers and films were observed using SEM (NanoSEM 200, FEI, Eindhoven, The Netherlands) after incubation for 3 days. The cells growing on nanofibers or films were washed with PBS and immersed in a 2 % (v/v) glutaraldehyde solution at 4 ± 1 °C for 4 h, then soaked with 20 %, 40 %, 60 %, 80 % (v/v), and absolute ethanol for 20 min.

2.13. Statistical analysis

All quantitative results were obtained from at least three samples and three independent experiments, with all the parameters reported as mean value and its standard deviation. Data analysis and visualization were performed in RStudio 2024.12.1 Build 563 (Posit Software, USA). Differences were analyzed using two-way (type of material and its composition; if other is not mentioned) analysis of variance (ANOVA) and the Tukey test for honestly significant differences at a significance level of $p = 0.05$.

3. Results and discussion

3.1. Film casting and nanofiber electrospinning

For nanofiber electrospinning, a set of input parameters, namely blend conductivity and viscosity, was tested to evaluate its effect on fiber and network structure (Fig.S1, Fig.S2). It was shown that the electrospinning of polymer blends with decreased conductivity allowed to obtain more homogeneous fibers without any beads and thickenings (Fig.S2c). In contrast, low viscosity of the polymer blend leads to spindle-shaped beads instead of nanofibers (Fig.S2d), while, its high viscosity promoted polymer chain entanglement, resulting in larger nanofibers (Fig.S2f). The viscosities of PVA/CSM/RR, PVA/CSM/RD and PVA/CSM/Au@RD NPs solutions were significantly lower compared to PVA/CSM one. This drop is a consequence of the addition of low-molecular-weight compounds, plant extracts, as well as Au

nanoparticles, which led to the weakening of contact and interactions between chains of PVA and CSM polymers in solution. It was reported that the morphology of electrospun nanofibers depends on blend conductivity, viscosity, and surface tension (Xue et al., 2019) so that making the electrospinning of polyelectrolyte blends challenging. In such a case, not viscosity, but rather repulsive forces between polyelectrolytes are the key factors limiting electrospinning. The electric field and polarity applied during electrospinning play a significant role regarding the surface properties of electrospun fibers (Stachewicz et al., 2012). When positive voltage is applied to a needle, electropositive functional groups of a polymer are repelled, and electronegative groups are aligned towards fiber surface. In blends and the used pH = 6, CSM possesses protonated amino groups (-NH_3^+), so that its chains are repelled from the fiber surface, resulting PVA chains (bearing electronegative -OH groups) ordering towards the surface. Thus, only when the viscosity reached a critical point of ~600 mPa×s, a homogeneous nanofiber structure was achieved. During the optimization process, the influence of surfactant was also examined, and the respected data is provided in Supplementary Materials as Chapter S1.

After completing the optimization of the electrospinning process, the applicable compositions of PVA/CSM-based blends and defined electrospinning parameters were implemented and are shown in Table 1 and Fig.S1. The highest value of conductivity was observed for the PVA/CSM blend, while the decreases were statistically significant for both PVA/CSM/RD, PVA/CSM/RR, and PVA/CSM/Au@RD NPs (Fig.S1a). Similarly, the addition of RD and RR aqueous extracts decreased blend viscosity in a statistically significant manner (Fig.S1b), still being acceptable for electrospinning.

For all the samples, electrospinning resulted in well-formed and smooth fibers with no visible defects. Moreover, the electrospun mats showed high uniformity in terms of fiber size distribution with a polydispersity index below 0.1 for all investigated nanofibers (Fig. 1).

The diameter of the PVA/CSM fibers and those with the addition of rose extracts (PVA/CSM/RD, PVA/CSM/RR) did not differ significantly and was determined to be *ca.* 105 nm (Fig. 1a-c). A slight increase was observed in the case of the addition of Au colloid to PVA/CSM blend (115 nm; Fig. 1d). Compositional changes affect the morphology of electrospun fibers, with the most prominent changes reported for PVA/CSM nanofibers, being determined by the component's ratio. The additives themselves, in the form of rose extracts or Au colloid, do not affect the quality and diameter of the obtained fibers under the same spinning conditions. This could be explained by the fact that their introduction even changes the solutions properties (conductivity, viscosity) but it still makes possible the electrospinning of homogeneous

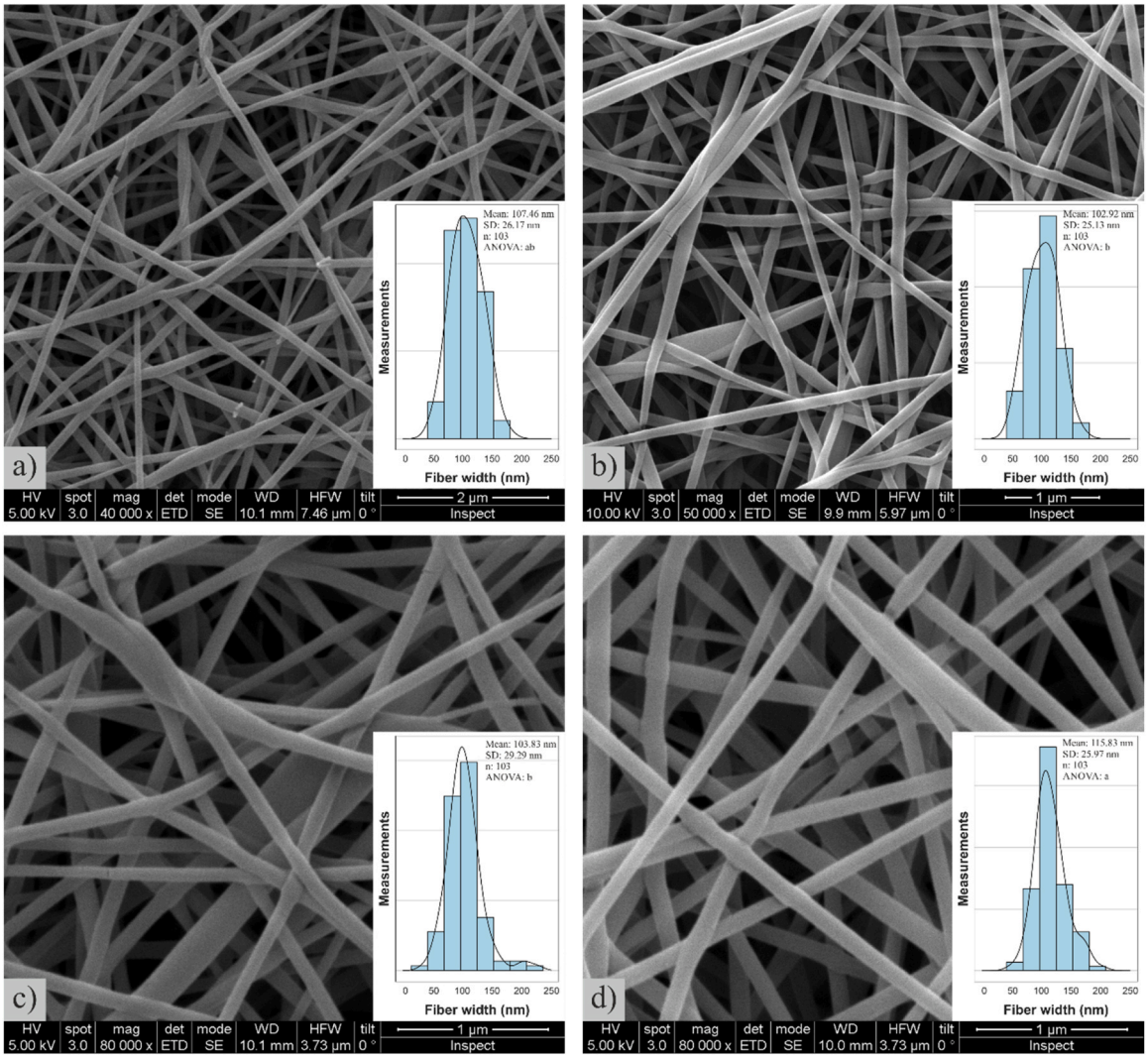

Fig. 1. Scanning electron microscopy images of PVA/CSM-based nanofibers: a) PVA/CSM sample; b) PVA/CSM/RD sample; c) PVA/CSM/RR sample; d) PVA/CSM/Au@RD NPs sample. Imaging parameters and scale bars are provided at the bottom of each specific subfigure. For each subfigure, a histogram of fiber width distribution is provided, as well as its statistical analysis. For one-way ANOVA, treatments with the same letter show a lack of statistically significant differences between the samples.

fibers (Table 1, Fig. S1, Fig. S2). Similarly, the applied thermal treatment at 130 °C for 1 h did not cause any significant changes in the morphology and size of the resulting nanofibers (Fig. S3).

3.2. Molecular properties

An averaged Raman spectra of PVA/CSM-based nanofibers and films are provided in the Supplementary Materials and shown in Fig.S7. Peaks corresponding to characteristic wavenumbers of structural bonds in CSM and PVA were observed, with detailed information on spectra interpretation provided in Table S1 of the Supplementary Materials. Due to the high degree of PVA hydrolysis, a band of residual acetate (at ~1708 cm^{-1}) showed low intensity. For PVA/CSM-based nanofibers and films with RR and RD additives, bands at 1600–1400 cm^{-1} and 1000–900 cm^{-1} can be assigned to aryl, alkenes and methyl groups of phenyl ethyl alcohol, citronellol, geraniol and nonadecane originating from rose extracts (Jentzsch et al., 2015). In all spectra, a broad band in the range of 3000–2800 cm^{-1} corresponds to hydroxyl group stretching vibrations of PVA, CSM, as well as phenolic compounds from RR and RD extracts, with its broad shape suggesting intra- and inter-molecular hydrogen bonding. To reduce data dimensionality, a graphical summary of the spectral changes in PVA/CSM-based nanofibers and films was obtained by evaluating the loadings of the principal components of the sample spectra. The PC1 versus PC2 scores plot (which describes approximately 48 % of the data variance) is shown in Fig. 2. For all sample groups, data showed the split into three major statistical groups – fibers, films, and control (CSM film). This is evidenced predominantly by the loadings of the PC2 component – positive for nanofibers and negative for films. Control CSM film shows both negative PC1 and PC2 loadings, in contrast to those of PVA/CSM-based samples, where PVA appears as the predominant component of both fibers and films. It was also observed that in terms of chemical composition, data variability is lower for PVA/CSM-based fibers, compared to the electrospun films, while the difference between specific sample groups showed the opposite trend. This suggests that PVA/CSM-based films are more structurally homogeneous, whereas the electrospun nanofibers are more similar in chemical composition.

3.3. Mechanical properties

As for the mechanical properties of PVA/CSN-based nanofibers and films, distinctive two-group data split was observed according to the sample type (nanofibers or films), with data represented in Fig. 3a. In case of PVA/CSM-based nanofibers, no statistically significant differences among samples were observed, with values ranging in between 0.04 and 0.25 GPa. Current values correspond to those reported previously (Bazzi et al., 2022), yet with no specific effect of the additives.

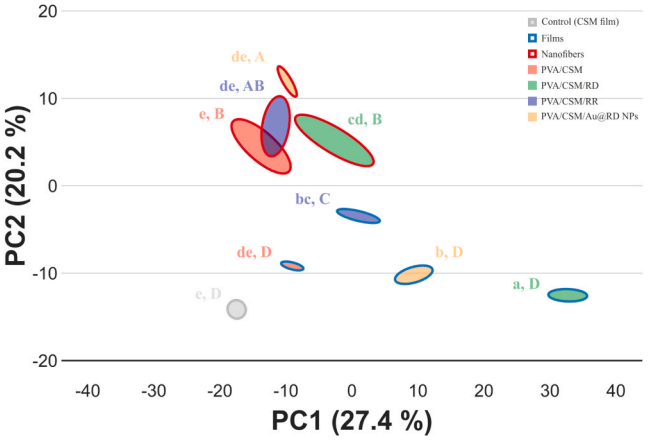

Fig. 2. Principal component (PC) analysis of PVA/CSM-based nanofibers and films. Principal component analysis of spectral data collected from PVA/CSM-based nanofibers and films showing a two dimensional score plot with average loadings of PC1 and PC2 for each type of sample. Data with different lower case and upper case letters have significantly different PC1 and PC2 values, respectively. The control sample (CSM film) is marked with the grey color.

In contrast, casted films with no rose extracts showed the highest Young's modulus of 2.75 ± 0.38 GPa. Current values are slightly higher than those reported previously, which can be a matter of reduced moisture content and storage conditions (Bonilla et al., 2014). In the case of casted films, statistically significant decrease of the Young's modulus was observed for the films with addition of rose extracts, which may be defined by the reduction of the intra- and inter-molecular hydrogen bonds network of CSM and PVA in favour of those of amine groups of chitosan and carbonyl groups of RD and RR flavonoids (Abdelghany et al., 2019). What is of high interest here, is that decrease of Young's modulus with an addition of Au@RD NPs is supposed to be not only the matter of the disintegration of hydrogen bond network, but also of the physical disruption of a fiber network, due to large NPs diameters, both physical (20.6 ± 2.7 nm) and hydrodynamic (85.0 ± 8.0 nm) (Kyzioł et al., 2021). Additionally, there was a clear reinforcing effect of PVA observed, as evidenced from data on mechanical properties of CSM-based films (Fig. S10a).

3.4. Wettability, swelling ability and degradation

Contact angle studies revealed that thermally stabilized samples of PVA/CSM-based nanofibers and films have a moderate hydrophilic surface (Fig. 4a). The average contact angle of PVA/CSM-based nanofibers was in the range of 35–45° and corresponds to the data reported previously (Liu et al., 2023). The current parameter is considered as crucial in terms of the development of antibacterial materials as the hydrophilicity of the polymer matrix promotes interactions between eucaryotic/prokaryotic cells and surfaces, as well as enhances the antibacterial effect of biocidal components (RD, RR, Au@RD NPs) on its surface (Li et al., 2018). Statistically significant increase was observed for PVA/CSM/RR nanofibers, suggesting the presence of relatively high amounts of phenols and flavonoids in *Rosa rugosa* (Olech et al., 2017), which increase material hydrophobicity (Krysa et al., 2025).

Corresponding PVA/CSM-based films were characterized by statistically higher values of contact angle. It is suggested to be defined by smoother surface morphology of casted films, which limit the Wenzel effect. In addition, electrospinning may enhance more prominent surface exposition of hydroxyl groups due to the higher value of surface area of electrospun nanofibers, compared to casted films (Ding et al., 2006). In the case of PVA/CSM/Au@RD NPs films, incorporation of Au@RD NPs resulted in the highest increase of sample hydrophobicity, which was confirmed by the statistically significant increase of contact angle value to 68.46 ± 8.75°. Such an effect related to the introduction of Au@RD NPs to fibrous materials has not been observed previously, but is supposed to correspond to nanoparticle size, shape and surface distribution patterns (Spano et al., 2012). While changes in polar surface free energy (Fig. 4b) of PVA/CSM-based nanofibers and films were opposite to the wettability pattern, dispersive surface free energy (Fig. 4c) followed its pattern.

Swelling ability and weight loss of PVA/CSM-based nanofibers and films as a function of incubation time is presented in Fig. 5. Swelling abilities of both PVA/CSM-based nanofibers and films shared the same pattern – rapid hydration up to 110–140 % of its initial mass, followed by a plateau (Figs. 5a, 5b). Compositional differences contributed to data variability the most, reporting PVA/CSM to show the highest swelling ability. It was assumed that the components of a RR and RD, possibly phenols and flavonoids, could suppress moisture uptake, assumingly interfering hydrogen bond network. It may be also indirectly confirmed with an increasing swelling ability of PVA/CSM/RR and PVA/CSM/RD nanofibers and films, suggesting rearrangement of the

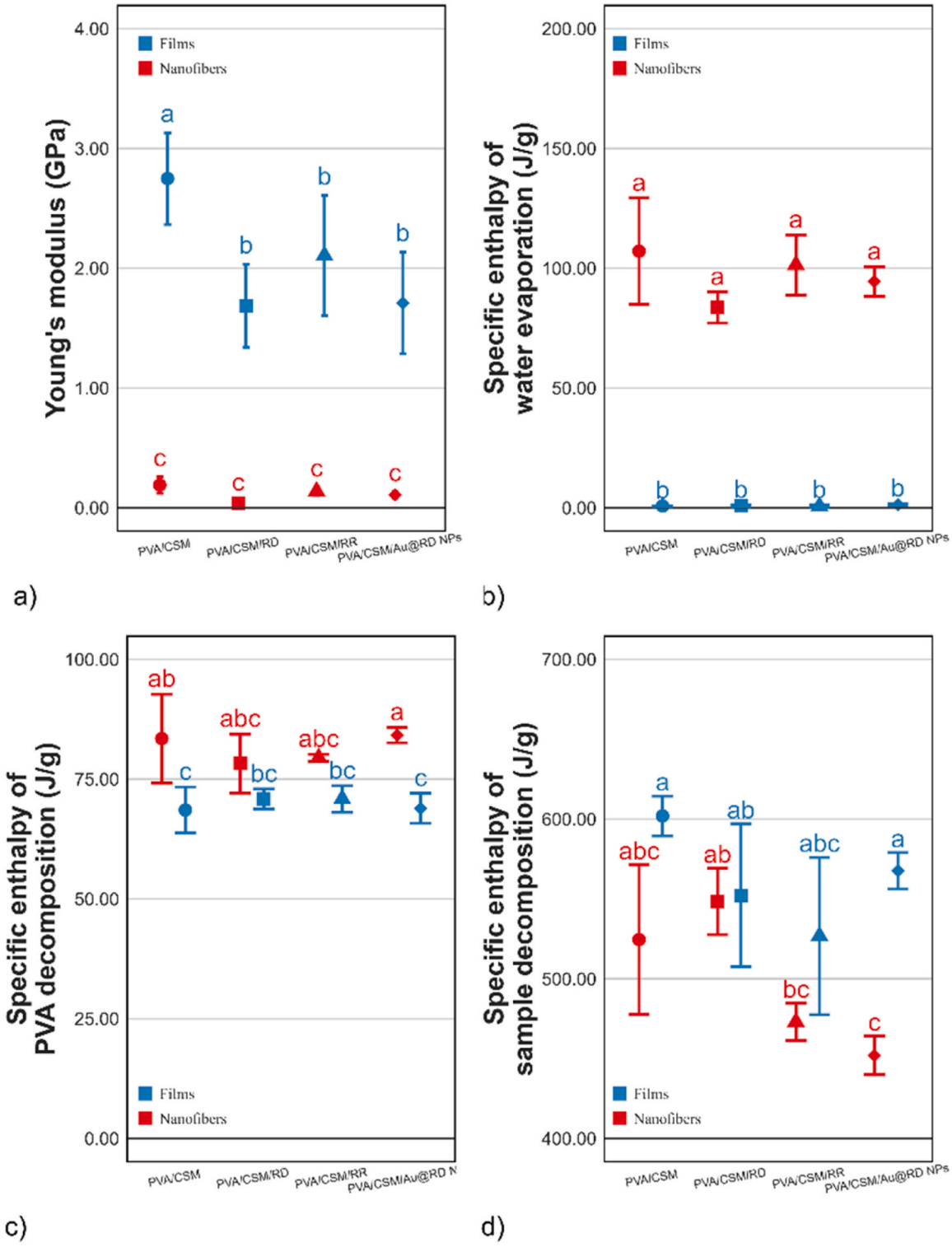

Fig. 3. Mechanical and thermal properties of PVA/CSM-based nanofibers and films: a) Young's modulus; b) specific enthalpy of water evaporation; c) specific enthalpy of PVA decomposition; d) specific enthalpy of sample decomposition. Treatments with the same letter show a lack of statistically significant differences between the samples. For subfigures b-d, respected peak temperatures are provided in supplementary Materials as fig. S8.

hydrogen bonding network by the buffer absorption. In turn, degradation kinetics followed the trends of previously reported data (Fathi et al., 2020), while differing as a matter of a sample form-factor. As far as no statistically significant differences in weight loss for PVA/CSM-based nanofibers and films as a matter of incubation time were observed (Fig. 5c), degradation was on average slower for PVA/CSM/RD and PVA/CSM/RR casted films (Fig. 5d).

3.5. *Thermal properties*

Obtained thermograms showed broad endothermic peak ranging maximum from 45 to 50 °C, and 75–80 °C for casted films and electrospun nanofibers, respectively, attributed to water evaporation (Fig. S8a). It is common for CSM-based materials due to hydrogen bond interactions between water and hydroxyl/amino groups of chitosan

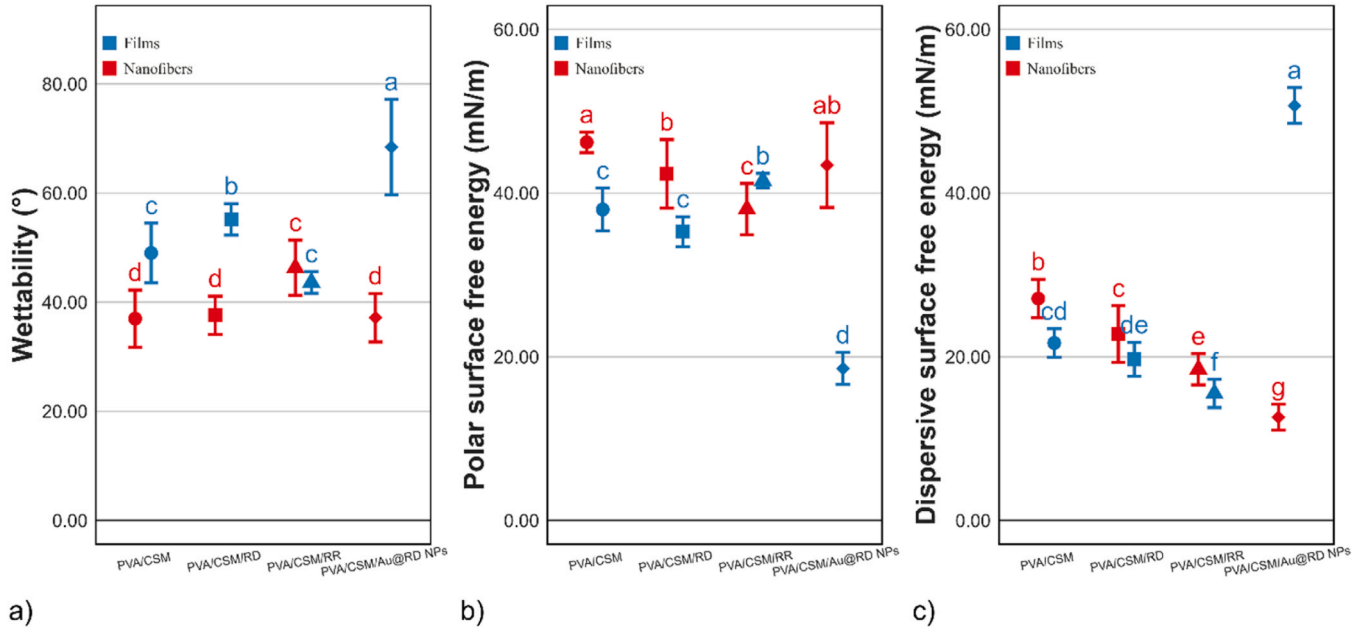

Fig. 4. Goniometric characterisation of thermally stabilized PVA/CSM-based nanofibers and films: a) wettability; b) polar surface free energy; c) dispersive surface free energy. Treatments with the same letter show a lack of statistically significant differences between the samples.

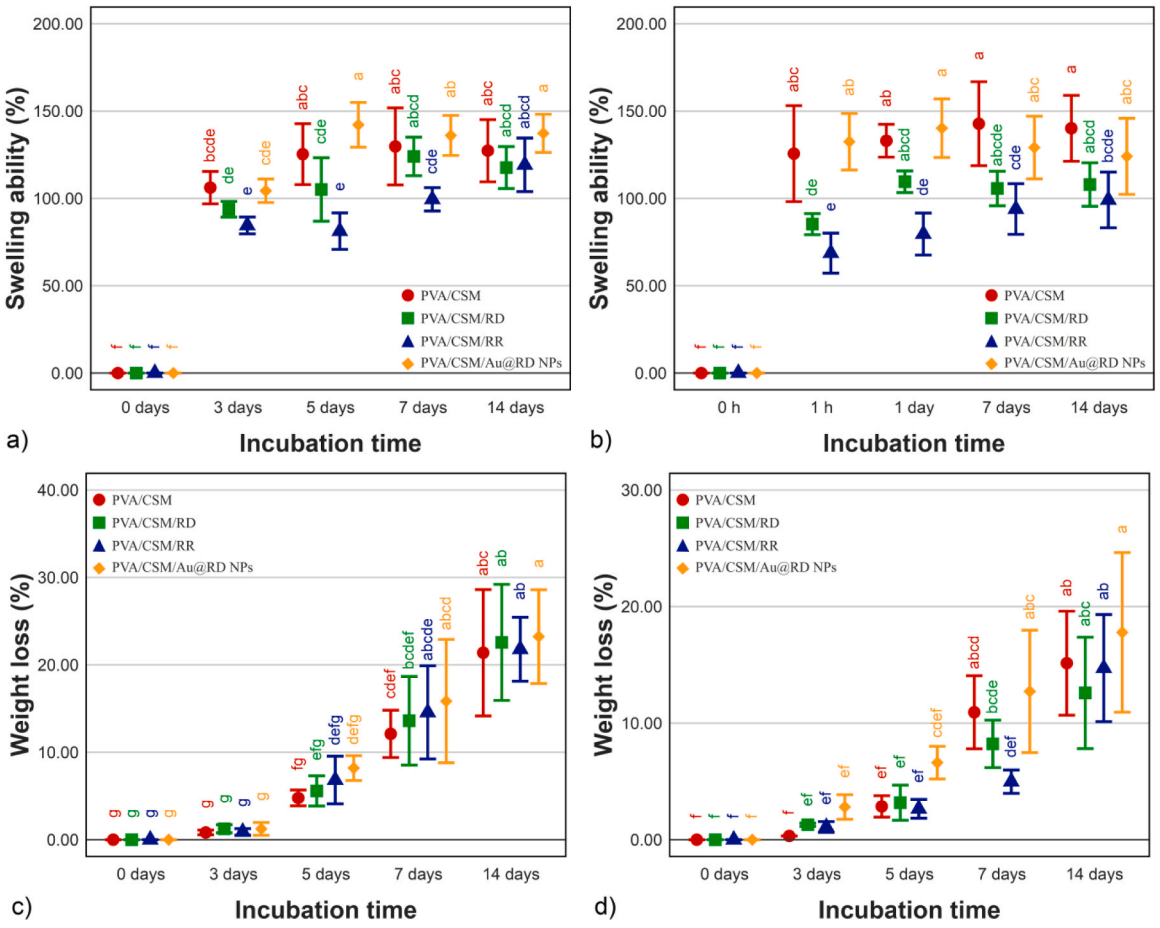

Fig. 5. Evaluation of swelling and degradation kinetics of thermally stabilized PVA/CSM-based nanofibers and films: a) swelling ability of electrospun nanofibers; b) swelling ability of casted films; c) weight loss of electrospun fibers; d) weight loss of casted films. Treatments with the same letter show a lack of statistically significant differences between the samples.

(Vargas et al., 2011). As for specific enthalpy of water evaporation, data for fibers were statistically higher, compared to casted films, with no difference as a matter of sample composition (Fig. 3b). It can be defined by higher polymer crystallinity in PVA/CSM-based electrospun nanofibers, as well as stronger hydrogen bonding of porous nanofiber network (Enayati et al., 2016). After removing physically bonded water, PVA/CSM-based nanofibers and films exhibited considerable thermal stability. At the 220–230 °C range (Fig.S8b) the samples showed an extra endothermal peak attributed to the PVA melting point (Nakano et al., 2007). Specific enthalpy of PVA melting was also in a narrow range of 60–90 J/g, with statistically significant data fluctuation regarding sample form-factor, and a moderate one as a matter of sample composition (Fig. 3c). Further on, the samples showed an exothermal peak of decomposition around 290–340 °C (Fig.S8c), which is in touch with the data, reported previously (John et al., 2017). It is assumed that PVA shifts peak temperatures and specific enthalpies of material decomposition to some higher values, supposedly by stabilizing interactions between glucosamine units (Casey and Wilson, 2015). The differences in specific enthalpy of sample degradation (Fig. 3d) may presumably be a matter of sample porosity and surface area, as for the electrospun nanofibers decomposition rate may be faster, compared to casted films. Relatively high thermal stability of biomaterials, reported in the current study, may be beneficial to address specific aspects of its practical use, namely stability during sterilization, retention of an *in vitro* stability, *etc.*. Noteworthy, the thermal stabilization of the investigated films and fibers the crystallinity of the resulting blends increased significantly implying that the stability also would increase in aqueous media (Table S2). As for the comparative analysis of CSM and PVA/CSM-based nanofilms and fibers (Fig. S10), addition of PVA limited moisture uptake of a material (Fig. S10b), as well as improved its thermal stability (Fig. S10c).

3.6. Antioxidant activity and in vitro biocompatibility

Antioxidant activity of PVA/CSM-based nanofibers and films is shown in Fig. 6a. The highest DPPH scavenging activity was exhibited by rose extracts (RD, RR) as controls, which correspond to data reported (Xie et al., 2022). Predominant mechanisms of RR and RD antioxidant activity lie in single electron and hydrogen atom transfers (Kim et al., 2022). In contrast, Au@RD NPs showed scavenging activity at a relatively low level (comparable to those of PVA/CSM-based nanofibers and films), so that flavonoids, glycosides and phenols of rose extracts determine the main antioxidant capabilities of nanofibers and films studied (El-Borady et al., 2023). The latter have shown a statistically significant increase of scavenging activity for PVA/CSM/RR, and PVA/CSM/RD samples, compared to PVA/CSM nanofibers and films. In contrast, a moderate increase in scavenging activity for PVA/CSM/Au@RD NPs was rather a plausible additive effect of its separate components.

The viability of HaCaT cells, grown on PVA/CSM-based nanofibers

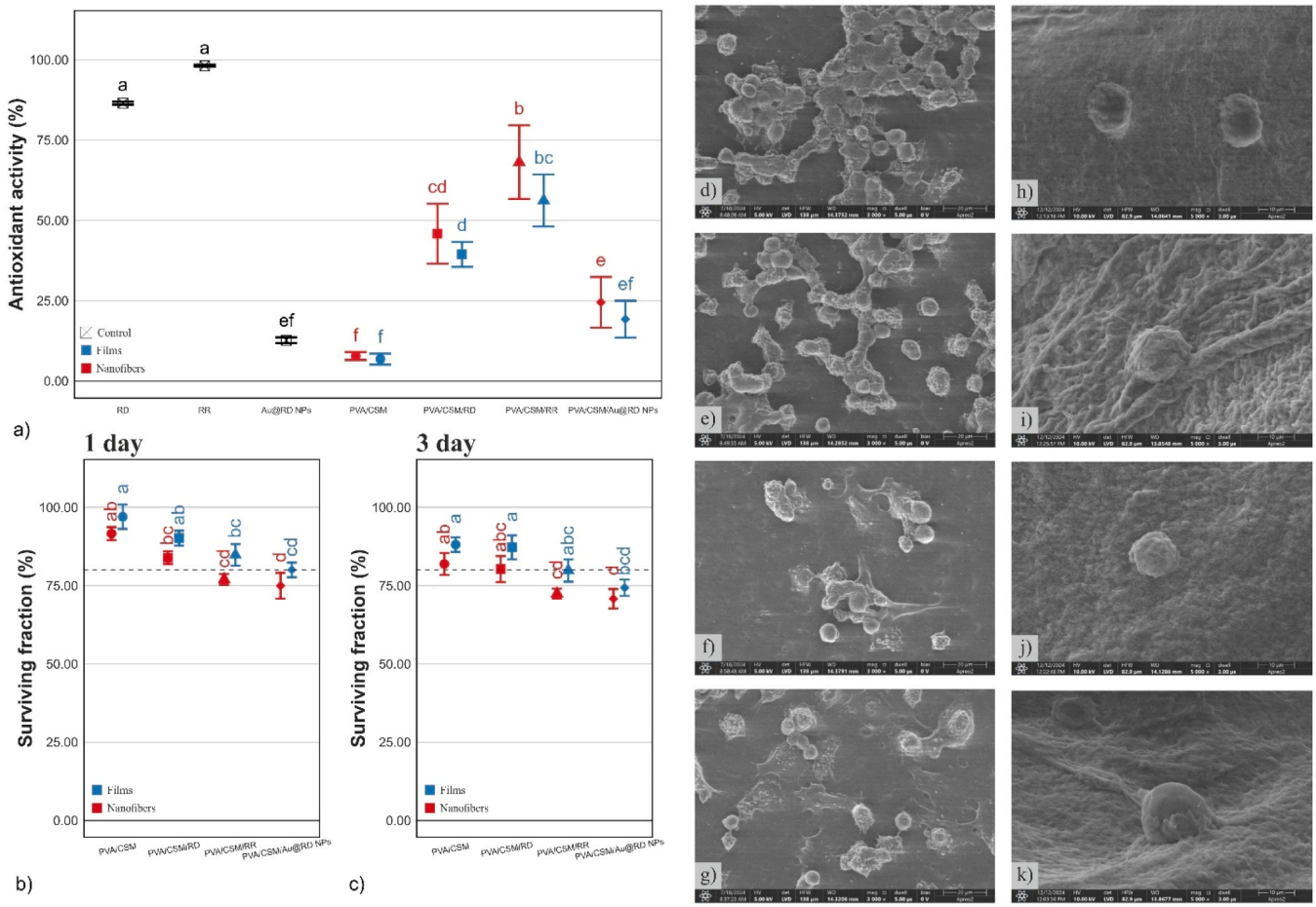

Fig. 6. Antioxidant and biological activities of PVA/CSM-based nanofibers and films: a) antioxidant activity; b) surviving fraction for HaCaT cells determined after 1 day of cell incubation; c) surviving fraction for HaCaT cells determined after 3 days of cell incubation. Subfigures d-k represent SEM images of the fixed HaCaT cells after 3 days of incubation on PVA/CSM-based casted films (d-g) and electrospun nanofibers (I-k): d, h) PVA/CSM; e, I) PVA/CSM/RD; f, j) PVA/CSM/RR; g, k) PVA/CSM/Au@RD NPs. for subfigures a-c, treatments with the same letter show lack of statistically significant differences between the samples, while for subfigures b-c, values above 80 % (dashed line) define lack of acute cytotoxicity.

and films is shown in Fig. 6b and Fig. 6c. Viability decreased with an addition of rose extracts, yet still not causing significant alterations in the cell surviving rate. It allows to consider current biomaterials as biocompatible in accordance with ISO 10993–5 standard (Tests for in vitro toxicity, 2009). In addition, there was a statistically significant decrease in surviving fraction percentage as a matter of duration (Fig. S9), with a less prominent trend for both nanofibers and films with an addition of rose extracts. This confirms the adhesion of cells to the surface and indicates their proper proliferation.

Additionally, cell morphology, viability and proliferation were examined by means of SEM (Figs. 6d-6k). Cells adhered to the sample surface confirming its proper proliferation. A dense monolayer of HaCaT cells was formed on PVA/CSM-based films (Figs. 6d-6g), while single cells were visible on respected nanofibers (Figs. 6h-6j). It corresponds to recent observations, reporting cells proliferation rate to be much higher for smooth surfaces, compared to rough (Huo et al., 2024). Apart from roughness, the wettability of the substrate is an essential factor for cell proliferation, affecting its adhesion, growth, survival, and intercellular communications (Morán et al., 2019). It was reported that a ~60 ° contact angle is an optimum for eucaryotic cells to adhere and grow of on smooth surfaces (Lv et al., 2018). In our case, the highest cell adhesion was achieved by the combined effect of moderate hydrophilicity and lack of surface roughness, while a limited cell adhesion was reported for hydrophilic nanofiber networks (Fig. 4a). Moreover, it is suggested that cell adhesion to nanofiber surface was in general weaker, as multi-step sample washing for SEM imaging was applied, removing loosely attached HaCaT cells. In addition, most of the cells grown on hydrophilic nanofiber networks were round-shaped, while those grown on PVA/CSM-based films surfaces displayed a better spread appearance.

3.7. *In vitro antibacterial activity*

In line with the aforementioned findings, further studies including exploration of antimicrobial activity of CSM-based casted films with rose extracts, gold nanoparticles, and selected antibiotics were carried out. According to preliminary studies, PVA-based casted films and

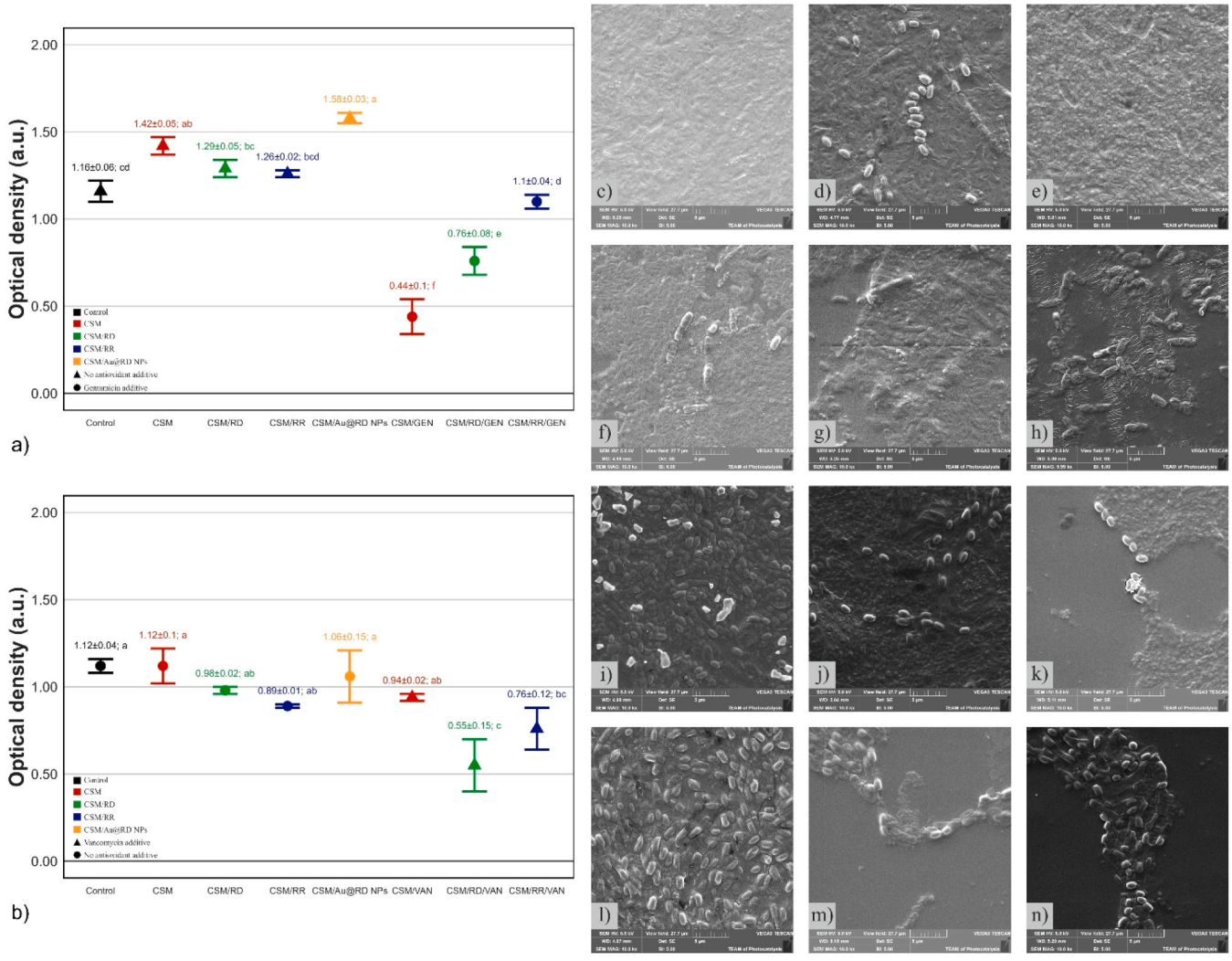

Fig. 7. Determination of antibacterial activities of CSM-based films against bacterial strains. Measurement of optical density at 600 nm (indirect contact method): a) Gram-negative *escherichia coli (dh5α)*; b) Gram-positive *bacillus paramycoides (op311)*. subfigures c)-n) represent SEM images of the *DH5α* (c)-h)) and *OP311* (I)-n)) bacteria strains on the surface of CSM-based casted films after 1 day of incubation on lysogeny broth agar plates (direct contact method): c) CSM; d) CSM/RD; e) CSM/RR; f) CSM/Au@RD NPs; g) CSM/RD/VAN; h) CSM/RR/VAN; I) CSM; j) CSM/RD; k) CSM/RR; l) CSM/Au@RD NPs; m) CSM/RD/VAN; n) CSM/RR/VAN. For subfigures a-b, antibacterial activity was evaluated by determining an optical density of lysogeny broth, with lower values responding to higher activity. Data on optical density are provided on figure as mean values with standard deviation. Treatments with the same letter show a lack of statistically significant differences between the samples. Differences were analyzed using one-way (medium constituents) analysis of variance (ANOVA) and the tukey test for honestly significant differences at a significance level of $p = 0.05$. for subfigures c-n, imaging parameters and scale bar are provided at the bottom of each specific subfigure. Material preparation, as well as methodology on antibacterial activity determination is provided in supplementary Materials as chapter S2.

electrospun nanofibers showed a lack of adhesion for the direct contact test on agar, while showing a lack of any bacteriostatic/bactericidal effect *in vitro* direct contact test in broth. In addition, the introduction of antibiotics (gentamicin, vancomycin) to current materials may serve as a promising introduction to the research on the effects of additivity/synergy of bioactive plant extracts and antibiotics. As evidenced by the data, rose extract additives resulted in a moderate yet statistically significant bacteriostatic effect to Gram-positive *OP311* bacteria strain, compared to bare CSM and control (Fig. 7b). It can be a matter of flavonoid incorporation into bacteria cellular membrane, as well as suppressing its DNA/RNA synthesis (Cendrowski et al., 2020). In contrast, no bacteriostatic effect to Gram-negative *DH5α* bacteria strain was reported for CSM-based films with the rose extract additives (Fig. 7a). It is supposed to be a matter of the presence of lipopolysaccharide extracellular membrane of *DH5α* bacteria strain, acting as a physical barrier for flavonoids and polyphenols of rose extracts. However, the integrity of the extracellular membrane of *DH5α* bacteria strain is supposed to be a matter of flavonoid and polyphenol concentrations in the rose extracts (Zhou et al., 2020).

In order not to increase the concentration of extracts, which would be associated with increased toxicity, it was decided to use the addition of antibiotics, selectively dedicated to Gram-negative (gentamicin) and Gram-positive (vancomycin) bacteria. It can be assumed that this approach would be beneficial due to the additive or synergic effects between these two components. This is also very valuable due to the potential possibility of reducing the overused antibiotic doses, so that the bacteria will not develop resistance mechanisms or will develop one at a slower rate. As suggested, the presence of gentamicin resulted in a statistically significant antibacterial activity for the Gram-negative *DH5α* strain, while vancomycin revealed the one activity for the Gram-positive *OP311* strain. Such activities correspond to those reported previously (Hodiamont et al., 2022). Noteworthy, the significant decrease in OD values can be observed in the case of the CSM/RD/VAN film (0.553 ± 0.145) compared to CSM/VAN (0.942 ± 0.020) for the Gram-positive *OP311* bacteria strain (Fig. 7b). The aforementioned data was confirmed with the results of SEM imaging (Fig. 7c-n), so that extensive bacteria-free regions were formed for CSM-based films with vancomycin and rose extracts (CSM/RD/VAN, CSM/RR/VAN) incubated on lysogeny broth agar plates with *OP311* bacteria strain (Fig. 7m-n). Noteworthy, in the case of both strains (*DH5α* and *OP311*), a statistically significant difference was observed in the antibacterial activity in the case of the rose extracts mixed with appropriate antibiotics when compared to extracts alone (both direct and indirect contact approaches; Fig. 7a, Fig. 7b). These results are very promising and further researches are required on the additive/synergetic effect of these components as reducing the doses of used antibiotics, especially in the current strategy to combat antibiotic-resistant bacteria strains.

4. Conclusions

In this study, the exploration of sample wettability, swelling ability, molecular, thermal and mechanical properties, supported by the cytotoxicity and antimicrobial activity studies allowed to estimate the role of material composition and fabrication technique on overall physicochemical properties and *in vitro* biological activity of the resulting materials of different nano-dimensionality: casted films (2D) and electrospun nanofibers (1D).

Results have shown that PVA/CSM-based blends require strict compositional and conditional settings to be spinnable, determined by the polyelectrolytes it is composed of. Despite similarities in blend composition, the fabrication technique defined structural homogeneity of PVA/CSM-based casted films, while electrospun nanofibers were closer in chemical composition. Noteworthy, the addition of rose extracts and Au@RD NPs to the composition of PVA/CSM-based films caused a decrease in their Young modulus, possibly due to the rearrangement of the PVA-CSM hydrogen bonding network. In addition, the fabrication technique highly affected the thermal properties of PVA/CSM-based films and nanofibers, with the high surface area of the latter resulting in higher moisture uptake and lower thermal stability. However, components of rose extracts (flavonoids, phenols) limit the swelling ability of PVA/CSM-based nanofibers and films, interfering with the hydrogen bond network.

Moreover, the current study supports an idea of Wenzel effect as a crucial determinant of PVA/CSM-based nanofiber wettability, affecting cell morphology, viability and proliferation. The addition of RD and RR extracts positively affected the antioxidant activity of PVA/CSM-based nanofibers and films, while the effect of Au@RD NPs was supposedly additive. The addition of both RD and RR extracts, as well as Au@RD NPs moderately decreased HaCaT cell viability, yet still not causing significant alterations in the cell survival rate and not showing acute cytotoxicity. In turn, statistically significant antibacterial activity was proved for CSM films with mixtures of rose extracts and the appropriate antibiotics. The most considerable effect was observed for the CSM/RD/VAN film in the case of the Gram-positive *OP311* bacteria strain.

All the data indicated above, as well as its thorough analysis, allow us to consider chitosan-poly(vinyl alcohol) casted films and electrospun nanofibers with the addition of RD and RR, as well as Au@RD NPs as promising biocompatible biomaterials, finding their potential applications in wound healing applications, tissue engineering, food packaging and beauty industry products.

CRediT authorship contribution statement

Agnieszka Kyzioł: Writing – review & editing, Writing – original draft, Visualization, Supervision, Methodology, Investigation, Funding acquisition, Formal analysis, Data curation, Conceptualization. **Julia Kulczyńska:** Writing – review & editing, Investigation, Data curation. Vadym Chibrikov: Writing – review & editing, Visualization, Methodology, Investigation, Formal analysis, Data curation. **Dominika Pawcenis:** Writing – review & editing, Investigation. **Victor Sebastian:** Writing – review & editing, Investigation. **Artur Zdunek:** Writing – review & editing, Methodology. **Roman J. Jędrzejczyk:** Writing – review & editing, Investigation. **Justyna Cybulska:** Writing – review & editing, Methodology, Investigation.

Declaration of Competing Interest

The authors declare that they have no known competing financial interests or personal relationships that could have appeared to influence the work reported in this paper.

Acknowledgements

This work was supported by the National Science Center within project OPUS 22 (2021/43/B/ST4/02833). Victor Sebastian acknowledges 2021–127847OB-I00 MCIN/AEI/10.13039/501100011033 and PDC2022–133866-I00 MCIN/AEI/10.13039/501100011033 (Unión Europea Next Generation EU/PRTR), the Severo Ochoa Programme for Centres of Excellence in R&D "Ayuda CEX2023–001286-S financiada por MICIU/AEI /10.13039/501100011033". Victor Sebastian also gratefully acknowledges CIBER-BBN, LMA-ELECMI and NANBIOSIS ICTs. The open-access publication of this article has been supported by a grant from the Faculty of Chemistry under the Strategic Programme Excellence Initiative at Jagiellonian University.

Appendix A. Supporting information

Supplementary data associated with this article can be found in the online version at doi:10.1016/j.indcrop.2025.121335.

Data availability

Data will be made available on request.

References

Abdelghany, A.M., Menazea, A.A., Ismail, A.M., 2019. Synthesis, characterization and antimicrobial activity of Chitosan/Polyvinyl alcohol blend doped with hibiscus sabdariffa L. Extract. J. Mol. Struct. 1197, 603–609. https://doi.org/10.1016/j.molstruc.2019.07.089.

Akram, M., et al., 2020. Chemical constituents, experimental and clinical pharmacology of rosa damascena: a literature review. J. Pharm. Pharmacol. 72 (2), 161–174. https://doi.org/10.1111/jphp.13185.

Alotaibi, B.S., et al., 2023. Development of Poly(vinyl alcohol)-Chitosan composite nanofibers for dual drug therapy of wounds. ACS Omega. https://doi.org/10.1021/acsomega.3c08856.

Amiri, N., et al., 2020. Teicoplanin-loaded chitosan-PEO nanofibers for local antibiotic delivery and wound healing. Int J. Biol. Macromol. 162, 645–656. https://doi.org/10.1016/j.ijbiomac.2020.06.195.

Bazzi, M., Shabani, I., Mohandesi, J.A., 2022. Enhanced mechanical properties and electrical conductivity of Chitosan/Polyvinyl alcohol electrospun nanofibers by incorporation of graphene nanoplatelets. no. November 2021, p J. Mech. Behav. Biomed. Mater. 125, 104975. https://doi.org/10.1016/j.jmbbm.2021.104975.

Bonilla, J., Fortunati, E., Atarés, L., Chiralt, A., Kenny, J.M., 2014. Physical, structural and antimicrobial properties of poly vinyl alcohol-chitosan biodegradable films. Food Hydrocoll. 35, 463–470. https://doi.org/10.1016/j.foodhyd.2013.07.002.

Budiarso, I.J., Rini, N.D.W., Tsalsabila, A., Birowosuto, M.D., Wibowo, A., 2023. Chitosan-Based smart biomaterials for biomedical applications: progress and perspectives. ACS Biomater. Sci. Eng. 9 (6), 3084–3115. https://doi.org/10.1021/acsbiomaterials.3c00216.

Casey, L.S., Wilson, L.D., 2015. Investigation of chitosan-PVA composite films and their adsorption properties (no. April). Int. Conf. Environ. Pollut. Public Health EPPH 2015, 78–84. https://doi.org/10.4236/gep.2015.32013.

Cendrowski, A., Krasniewska, K., Przybył, J.L., Zielinska, A., Kalisz, S., 2020. Antibacterial and antioxidant activity of extracts from rose fruits (Rosa rugosa). Molecules 25 (6). https://doi.org/10.3390/molecules25061365.

Chibrikov, V., Pieczywek, P.M., Cybulska, J., Zdunek, A., 2023. Evaluation of elasto-plastic properties of bacterial cellulose-hemicellulose composite films (no. December, p). Ind. Crops Prod. 205, 117578. https://doi.org/10.1016/j.indcrop.2023.117578.

Chuah, L.H., Loo, H.L., Goh, C.F., Fu, J.Y., Ng, S.F., 2023. Chitosan-based drug delivery systems for skin atopic dermatitis: recent advancements and patent trends. Drug Deliv. Transl. Res 13 (5), 1436–1455. https://doi.org/10.1007/s13346-023-01307-w.

Ding, B., Li, C., Hotta, Y., Kim, J., Kuwaki, O., Shiratori, S., 2006. Conversion of an electrospun nanofibrous cellulose acetate mat from a super-hydrophilic to super-hydrophobic surface. Nanotechnology 17 (17), 4332–4339. https://doi.org/10.1088/0957-4484/17/17/009.

El-Borady, O.M., Fawzy, M., Hosny, M., 2023. Antioxidant, anticancer and enhanced photocatalytic potentials of gold nanoparticles biosynthesized by common reed leaf extract. Appl. Nanosci. (Switz.) 13 (5), 3149–3160. https://doi.org/10.1007/s13204-021-01776-w.

Enayati, M.S., et al., 2016. Crystallinity study of electrospun poly (vinyl alcohol) nanofibers: effect of electrospinning, filler incorporation, and heat treatment. Iran. Polym. J. (Engl. Ed.) 25 (7), 647–659. https://doi.org/10.1007/s13726-016-0455-3.

Fathi, A., et al., 2020. Fabrication of chitosan-polyvinyl alcohol and silk electrospun fiber seeded with differentiated keratinocyte for skin tissue regeneration in animal wound model. J. Biol. Eng. 14 (1), 1–14. https://doi.org/10.1186/s13036-020-00249-y.

Garnica-Palafox, I.M., Sánchez-Arévalo, F.M., 2016. Influence of natural and synthetic crosslinking reagents on the structural and mechanical properties of chitosan-based hybrid hydrogels. Carbohydr. Polym. 151, 1073–1081. https://doi.org/10.1016/j.carbpol.2016.06.036.

Hodiamont, C.J., van den Broek, A.K., de Vroom, S.L., Prins, J.M., Mathôt, R.A.A., van Hest, R.M., 2022. Clinical pharmacokinetics of gentamicin in various patient populations and consequences for optimal dosing for Gram-Negative infections: an updated review. Clin. Pharm. 61 (8), 1075–1094. https://doi.org/10.1007/s40262-022-01143-0.

Huo, Z., et al., 2024. Biomechanics of macrophages on disordered surface nanotopography. ACS Appl. Mater. Interfaces 16 (21), 27164–27176. https://doi.org/10.1021/acsami.4c04330.

Javed, Z., et al., 2023. Examining current research trends in ozone formation sensitivity: a bibliometric analysis. Processes 11 (8). https://doi.org/10.3390/pr11082240.

Jentzsch, P.V., Ramos, L.A., Ciobotă, V., 2015. Handheld Raman spectroscopy for the distinction of essential oils used in the cosmetics industry. Cosmetics 2 (2), 162–176. https://doi.org/10.3390/cosmetics2020162.

John, S., Joseph, A., Kuruvilla, M., Sajini, S., 2017. Inhibition of mild steel corrosion using Chitosan–Polyvinyl alcohol nanocomposite films by Sol–Gel method: an environmentally friendly approach. J. Bio Tribocorros 3 (1), 1–9. https://doi.org/10.1007/s40735-016-0062-z.

Kikani, T., Thale, R., Thakore, S., 2024. On-Demand removable chitosan based self-healing and antibacterial hydrogel for delivery of tetracycline and curcumin as potential wound dressing material. ACS Appl. Bio Mater. https://doi.org/10.1021/acsabm.4c00680.

Kim, E., Mok, H.K., Hyun, T.K., 2022. Variations in the antioxidant, anticancer, and anti-inflammatory properties of different rosa rugosa organ extracts. Agronomy 12 (2). https://doi.org/10.3390/agronomy12020238.

Krajewska, B., Wydro, P., Jańczyk, A., 2011. Probing the modes of antibacterial activity of chitosan. Effects of ph and molecular weight on chitosan interactions with membrane lipids in langmuir films. Biomacromolecules 12 (11), 4144–4152. https://doi.org/10.1021/bm2012295.

Krysa, M., et al., 2025. The effect of surface adsorption of caffeic, chlorogenic, and gallic acids on the properties of cellulose- and nanocellulose-based films. no. December 2024 Ind. Crops Prod. 224. https://doi.org/10.1016/j.indcrop.2024.120349.

Kulkarni, A.D., et al., 2017. Xyloglucan: a functional biomacromolecule for drug delivery applications. Int J. Biol. Macromol. 104, 799–812. https://doi.org/10.1016/j.ijbiomac.2017.06.088.

Kyzioł, A., et al., Jan. 2021. Towards plant-mediated chemistry – au nanoparticles obtained using aqueous extract of rosa damascena and their biological activity in vitro. J. Inorg. Biochem 214, 111300. https://doi.org/10.1016/j.jinorgbio.2020.111300.

Li, M., Liu, X., Liu, N., Guo, Z., Singh, P.K., Fu, S., 2018. Effect of surface wettability on the antibacterial activity of nanocellulose-based material with quaternary ammonium groups (no. May). Colloids Surf. A Physicochem Eng. Asp. 554, 122–128. https://doi.org/10.1016/j.colsurfa.2018.06.031.

Liu, F., et al., 2023. Improved hydrophobicity, antibacterial and mechanical properties of polyvinyl alcohol/quaternary chitosan composite films for antibacterial packaging (no. March, p). Carbohydr. Polym. 312, 120755. https://doi.org/10.1016/j.carbpol.2023.120755.

Lv, L., et al., 2018. Unveiling the mechanism of surface hydrophilicity-modulated macrophage polarization. Adv. Health Mater. 7 (19), 1–11. https://doi.org/10.1002/adhm.201800675.

Martau, G.A., Mihai, M., Vodnar, D.C., 2019. The use of chitosan, alginate, and pectin in the biomedical and food sector—biocompatibility, bioadhesiveness, and biodegradability. Polym. (Basel) 11 (11), 1837. https://doi.org/10.3390/polym11111837.

Michalicha, A., Belcarz, A., Giannakoudakis, D.A., Staniszewska, M., Barczak, M., 2024. Designing composite stimuli-responsive hydrogels for wound healing applications: the state-of-the-art and recent discoveries. Materials 17 (2). https://doi.org/10.3390/ma17020278.

Mishra, Y., et al., 2022. Application of nanotechnology to herbal antioxidants as improved phytomedicine: an expanding horizon. Biomed. Pharmacother. 153. https://doi.org/10.1016/j.biopha.2022.113413.

Mohamady Hussein, M.A., Baños, F.G.D., Grinholc, M., Abo Dena, A.S., El-Sherbiny, I.M., Megahed, M., 2020. Exploring the physicochemical and antimicrobial properties of gold-chitosan hybrid nanoparticles composed of varying chitosan amounts. Int J. Biol. Macromol. 162, 1760–1769. https://doi.org/10.1016/j.ijbiomac.2020.08.046.

Morán, M.C., Ruano, G., Cirisano, F., Ferrari, M., 2019. Mammalian cell viability on hydrophobic and superhydrophobic fabrics. no. November 2018 Mater. Sci. Eng. C. 99, 241–247. https://doi.org/10.1016/j.msec.2019.01.088.

Nakano, Y., et al., 2007. Structure and mechanical properties of chitosan/poly(vinyl alcohol) blend films. Macromol. Symp. 258, 63–81. https://doi.org/10.1002/masy.200751208.

Natolino, A., Voce, S., Alò, E., Comuzzo, P., 2025. Exploring an eco-friendlier strategy for chitosan production and valuable compounds recovery from mushroom by-products with modified subcritical water. Innov. Food Sci. Emerg. Technol. 100, 103923. https://doi.org/10.1016/j.ifset.2025.103923.

Olech, M., et al., 2017. Multidirectional characterisation of chemical composition and health-promoting potential of rosa rugosa hips. Nat. Prod. Res 31 (6), 667–671. https://doi.org/10.1080/14786419.2016.1180601.

Perveen, S., et al., 2023. Utilization of biomaterials to develop the biodegradable food packaging. Int J. Food Prop. 26 (1), 1122–1139. https://doi.org/10.1080/10942912.2023.2200606.

Pinto, E.P., et al., 2018. Influence of low and high glycerol concentrations on wettability and flexibility of chitosan biofilms. Quim. Nova 41 (10), 1109–1116. https://doi.org/10.21577/0100-4042.20170287.

Rakkan, T., et al., 2025. Cellulose nanofiber-reinforced chitosan/PVA/MXene (Ti3C2Tx) membrane: enhanced multifunctional performance and non-cytotoxicity for drug delivery. Carbohydr. Polym. Technol. Appl. 9, 100712. https://doi.org/10.1016/j.carpta.2025.100712.

Spano, F., Massaro, A., Blasi, L., Malerba, M., Cingolani, R., Athanassiou, A., 2012. In situ formation and size control of gold nanoparticles into chitosan for nanocomposite surfaces with tailored wettability. Langmuir 28 (8), 3911–3917. https://doi.org/10.1021/la203893h.

Stachewicz, U., Stone, C.A., Willis, C.R., Barber, A.H., 2012. Charge assisted tailoring of chemical functionality at electrospun nanofiber surfaces. J. Mater. Chem. 22 (43), 22935–22941. https://doi.org/10.1039/c2jm33807f.

Sun, J., Perry, S.L., Schiffman, J.D., 2019. Electrospinning nanofibers from chitosan/hyaluronic acid complex coacervates. Biomacromolecules 20 (11), 4191–4198. https://doi.org/10.1021/acs.biomac.9b01072.

Taokaew, S., Chuenkaek, T., 2024. Developments of core / shell chitosan-based nanofibers by electrospinning techniques: a review (no). Fibers 12, 26. https://doi.org/10.3390/fib12030026.

Tests for in vitro toxicity," *in Biological Evaluation of Medical Devices*, no. 3, 2009. [Online]. Available: ⟨https://nhiso.com/wp-content/uploads/2018/05/ISO-10993-5-2009.pdf⟩.

Toker-Bayraktar, M., Erenay, B., Altun, B., Odabaş, S., Garipcan, B., 2023. Plant-derived biomaterials and scaffolds. Cellulose 30 (5), 2731–2751. https://doi.org/10.1007/s10570-023-05078-y.

United Nations, "The 17 Goals," Department of Economic and Social Affairs Sustainable Development. [Online]. Available: ⟨https://sdgs.un.org/goals⟩.

Vargas, M., Albors, A., Chiralt, A., González-Martínez, C., 2011. Water interactions and microstructure of chitosan-methylcellulose composite films as affected by ionic concentration. Lwt 44 (10), 2290–2295. https://doi.org/10.1016/j.lwt.2011.02.018.

Wang, H., 2024. Beneficial medicinal effects and material applications of rose. Heliyon 10 (1), e23530. https://doi.org/10.1016/j.heliyon.2023.e23530.

Wang, Y., Yu, Y., Shi, C., Ren, Y., Han, J., Wu, R., 2025. Development of curcumin nanoparticle-modified photodynamic gelatin/PVA–chitosan bilayer films for preserving bigeye tuna. Int J. Biol. Macromol. 308, 142299. https://doi.org/10.1016/j.ijbiomac.2025.142299.

Xie, J., Li, M.-X., Du, Z.-Z., 2022. Chemical compounds, anti-aging and antibacterial properties of rosa rugosa purple branch (no). Ind. Crops Prod. 181, 114814. https://doi.org/10.1016/j.indcrop.2022.114814.

Xu, J., Zhang, J., Gao, W., Liang, H., Wang, H., Li, J., 2009. Preparation of chitosan/PLA blend micro/nanofibers by electrospinning. Mater. Lett. 63 (8), 658–660. https://doi.org/10.1016/j.matlet.2008.12.014.

Xue, J., Wu, T., Dai, Y., Xia, Y., 2019. Electrospinning and electrospun nanofibers: methods, materials, and applications. Chem. Rev. 119 (8), 5298–5415. https://doi.org/10.1021/acs.chemrev.8b00593.

Zakrzewska, A., et al., 2023. Electrospun Poly(vinyl alcohol)-Based conductive Semi-interpenetrating polymer network fibrous hydrogel: a toolbox for optimal Cross-Linking. ACS Mater. Au 3 (5), 464–482. https://doi.org/10.1021/acsmaterialsau.3c00025.

Zhou, Y., et al., 2020. Antibacterial activity and mechanism of green tea polysaccharide conjugates against escherichia coli (no. January, p). Ind. Crops Prod. 152, 112464. https://doi.org/10.1016/j.indcrop.2020.112464.